A STUDY ON FREQUENCY RESPONSE FUNCTIONS IN PAVEMENT ENGINEERING

FILIPPO G. PRATICO[1], GIANFRANCO PELLICANO*[1], MATTEO BOLOGNESE[2], GAETANO LICITRA[2]

[1]*DIIES Department, University Mediterranea, Reggio Calabria, Italy*

[2]*Environmental Protection Agency of Tuscany Region, Pisa, Italy*

Abstract. Mechanical impedance (MI) defines the ability of a system to vibrate as a consequence of force application. In the recent years, the correlation of this parameter with tire-road noise and other characteristics has gained certain attention. Nevertheless, the information about this topic is still insufficient. Usually, the force is set through an impulse hammer as a master and the acceleration is measured through an accelerometer as a response in order to measure the corresponding Frequency Response Function (FRF). The objectives of the study presented in this paper are i) to analyse the differences between the axial mechanical impedance (complex ratio of force and velocity referred to the same point, named driving-point impedance) and the non-axial mechanical impedance (complex ratio of the force at the point *i* and velocity at the point *j*, named transfer impedance); ii) to analyse the effect of adding crumb rubber (2% by mixture weight) and of the percentage of bitumen on the mechanical impedance for the bituminous samples. Therefore, laboratory tests on asphalt concrete specimens have been performed, using an instrumentation system composed of i) an impact hammer reporting the impact force value; ii) an impedance head measuring the direct impact force and the direct acceleration

* Corresponding author. E-mail: gia.pellicano@gmail.com

Filippo G. PRATICO (ORCID ID 0000-0003-3576-7976)
Gianfranco PELLICANO (ORCID ID 0000-0003-2551-2603)
Matteo BOLOGNESE (ORCID ID 0000-0003-0460-1295)
Gaetano LICITRA (ORCID ID 0000-0003-4867-0954)

Filippo G. Pratico,
Gianfranco Pellicano,
Matteo Bolognese,
Gaetano Licitra

A study
on frequency
response functions
in pavement
engineering

at the hitting point location; iii) a piezoelectric accelerometer measuring the transfer acceleration at a certain distance from the hitting point location. Results demonstrate that the ratio between the repeatability and the average is quite constant, while for heights higher than 10 cm, also MI tends to be independent on the height. A number of recommendations have been made based on the results of the present research.

Keywords: crumb rubber, driving-point impedance, frequency response function, impact hammer, mechanical impedance, transfer impedance.

Introduction

Structures, structural elements, and materials can be investigated using forced vibration techniques (Olesen, 1977; Fedele et al., 2017) and frequency response functions (FRF), such as mechanical impedance (MI) and dynamic stiffness. In 1963, the American Standard USAS S2.6 defined mechanical impedance as "a quantitative measure of the ability of a structure to resist a vibratory force". The mechanical impedance of a structure, at any point, may be also defined as the ratio of a sinusoidal force applied to the structure to the resulting sinusoidal velocity in the direction of the force (Harris & Piersol, 2002). If force and motion are measured at the same point, the ratio is termed driving-point impedance. If force and motion are measured at different points (or the same point but with a different angle between them), the ratio is termed transfer impedance (Gerdeen, 1975; Hamet & Klein, 2004; Olesen & Randall, 1979). A property of a linear, time-invariant mechanical system is that at the same frequency, in case the excitation is a steady-state harmonic input, the response also appears to be a steady-state harmonic motion (Gatscher & Kawiecki, 1994). So, to describe the relationship between harmonic force and harmonic response, two parameters are required: the ratio of the magnitudes of the two harmonically varying quantities and the phase angle between them (Gatscher & Kawiecki, 1994).

To this end, it is noted (cf. Figure 1) that based on differential equations in the time domain (e.g., Equation (1)), under given boundary conditions (e.g., $v(0) = x(0) = 0$), the given system in the steady state can be described using the Laplace transform. This allows deriving the corresponding equations in the frequency domain in terms of mechanical impedance and receptance. For example,

$$f(t) = m\ddot{x} + c\dot{x} + kx, \tag{1}$$

$$F(s) = V(s)\left[ms + c + \frac{k}{s} \right], \tag{2}$$

where $s = j\omega$, $j=\sqrt{-1}$, m is the mass, $f(t)$ is the force over time, N, $F(s)$ in the force over frequencies, c is the viscous damping coefficient, N·s/m, k is the spring constant, N/m, while $\ddot{x}$, $\dot{x}$ and x are the acceleration, m/s², the speed, m/s and the displacement, m, respectively. Equation (3) can be derived (frequency domain, where $\omega = 2\pi f$) based on Equation (1) and Equation (2)

$$\frac{X(s)}{F(s)} = \frac{1}{ms^2 + cs + k}. \tag{3}$$

Note that the corresponding resonant (angular) frequency is given by $\omega_n = \sqrt{k/m}$.

Importantly, resonances correspond to valleys in Equation (2) and to peaks in Equation (3). It is noted that $f(t)$ (unit: N) frequency-domain forces, $F(s)$, are obtained from time-domain forces. In turn, $F(s)$ has units of Newton·seconds. Similarly, speeds in the time domain ($V(t)$) have units of m/s, while in the frequency domain ($V(s)$) have units of meters. For MI, because we need to divide forces by speeds, MI has the same unit of measure in both frequency and time domain. It should be noted that in Equation (2) for low angular frequencies, it is stiffness (i.e., N/m, k/ω) that governs, whereas for high angular frequencies, it is the mass ($m\cdot\omega$) that governs the equation (see Figure 1).
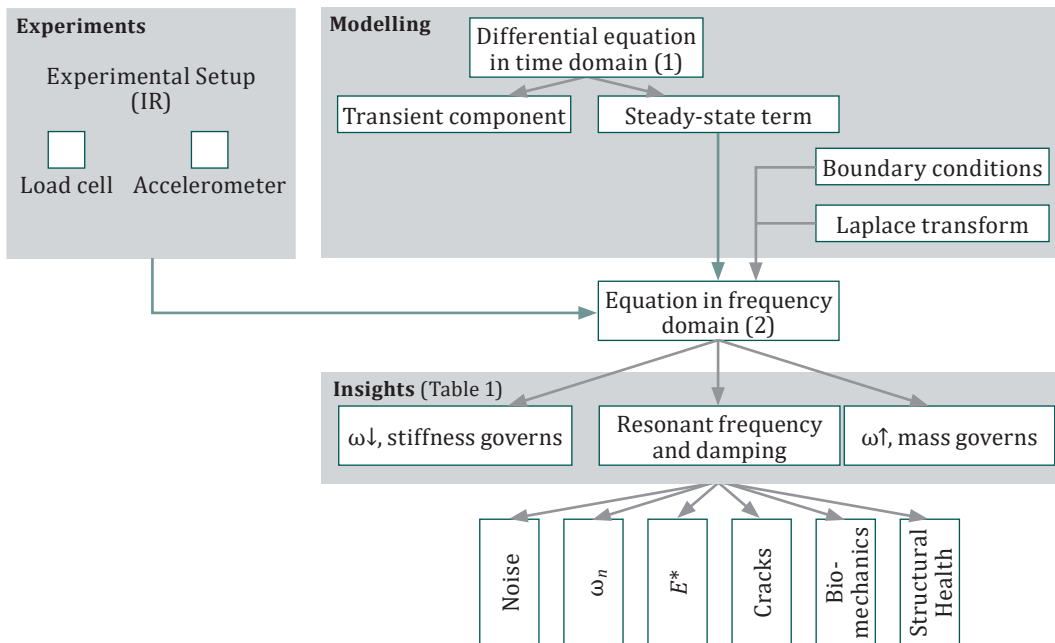
Figure 1. Model-based vs. experiment-based FRFs

Filippo G. Pratico,
Gianfranco Pellicano,
Matteo Bolognese,
Gaetano Licitra

A study
on frequency
response functions
in pavement
engineering

Importantly, the schematic in Figure 1 presents just pavement-related factors, while boundary conditions can also greatly affect the overall response. This also applies to pavement-tyre coupling where the effect depends not only on the pavement but also on the tyre. In other terms, it is acknowledged that, formally speaking, Figure 1 pertains to decoupling problems.

The Impulse Response (IR; cf. Figure 1) method is one of the most frequently used methods to derive the mechanical impedance. It is a non-destructive test (NDT), where the dynamic response of a structural element to an impact event (usually a hammer hit) is measured using an accelerometer or a geophone in order to evaluate the stiffness and integrity of the structure ((Clem et al., 2013), cf. Table 1).

In Table 1, some of the uses of the frequency response function (FRF) as described in the literature are summarized.

In their review, Brown et al. (2015) analyzed the principal issues that can influence the impact hammer testing. The force spectrum is affected by such factors as a certain characteristic of the removable tip used: a soft tip spreads the applied energy over a longer time period and thus gives a lower maximum frequency that can be used. A hard tip concentrates the applied energy over a shorter time period and thus gives a higher maximum frequency). Other factors include addition of a mass to the back of the impact hammer or giving different velocities to the hammer hit.

Gucunski et al. (2013) illustrated the possibility to use the impulse response method to detect concrete bridge deck deterioration. This NDT technology has proved to have good potential for delamination detection and characterization.

Pimentel et al. (2017) used the impact test to detect damages in reinforced concrete slabs: the crack-induced damage was monitored and evaluated by applying static loads on a slab built in the laboratory. Several modal tests were carried out using an impact hammer. The aim of the study was to evaluate the level of changes of the fundamental frequency along the decay after impacting the slab. It was observed that the gradient of the time-frequency curves throughout varied according to the level of cracking induced by the static load.

Shubert et al. (2010) focused on the impact of asphalt concrete on the resonant frequency of timber bridges.

In the study presented by Tlaisi et al. (2012), investigations were carried out in order to identify the existence of cracks in a shaft system using the mechanical impedance approach: impedance and mobility were measured and simulated in the vertical direction. The conclusion made in the study was that the amplitudes of all mobility curves increase for the resonant frequencies for increasing crack depth; in contrast, the

amplitudes of all impedance curves decrease at the first anti-resonance frequencies (or increase at the third anti-resonance frequencies) for increasing crack depths.

Czech and Gardziejczyk (2022) focused on the assessment of the dynamic stiffness of poroelastic and asphalt concretes. They found that poroelastic pavements have a much lower dynamic stiffness (138~143 dB re. 1 N/m) compared to asphalt concrete pavements (150 dB re. 1 N/m). They carried out experiments both on site and in the laboratory using an exciter.

Gil-Abarca et al. (2021) focused on rubberized bituminous mixtures using the non-resonant method and a vibration exciter (shaker). At 400 Hz they obtained the values of dynamic stiffness in the range 1.5×10^7~2.7×10^7 N/m, corresponding to 144~149 dB re. 1 N/m. Cesbron et al. (2021) addressed asphalt concretes for electric vehicles. Their measurements of dynamic stiffness resulted in values of about 160~165 dB re. 1 N/m.

In the last years, an increasing number of studies investigated the relationship between mechanical impedance and traffic noise.

During the PERSUADE project (Bendtsen et al., 2013), tests on poroelastic road surfaces (PERS) were performed in Arnakke (Denmark). The experimental setup was composed of a hammer delivering an impact force $f(t)$, an impedance head measuring the direct force $fd(t)$ and the direct acceleration $ad(t)$ at the impact location, and an accelerometer measuring the transfer acceleration $at(t)$ at a certain distance from the impact point. Finally, the driving-point impedance (called direct impedance by the authors) and the transfer impedance were calculated: for the whole frequency range, the transfer mechanical impedance resulted in the same shape but by 40 dB higher than the direct impedance. This was explained by the damping of the vibrations while they propagated into the poroelastic medium. It should be noted that in this case measurements were carried out on the road pavement.

Within the LIFE SOUNDLESS project (Morcillo et al., 2019), in order to improve the noise attenuation of pavements, different ways to modify stone mastic asphalt mixes were analyzed. The best mixtures were selected considering not only traditional mechanical parameters but also on the baiss of the dynamic stiffness and damping. It was concluded that the mechanical impedance was the most relevant parameter in selecting a quieter mixture.

Notably, within the LIFE E-VIA project, mixtures were produced with an aim to reduce noise and life cycle cost impact and FRFs were used on-site and in the laboratory. Similarly, noise- and vibration-oriented studies are in progress as a part of the project LIFE SNEAK, where

complex scenarios are going to be investigated (noise and vibrations deriving from rail tracks and roads).

Vázquez et al. (2015) carried out dynamic stiffness measurements on different bituminous mixtures using the Non-Resonant Method (i.e., where the sample ends cannot freely move). The experimental set-up involved a vibration exciter and an impedance head in contact with the surface of the sample tested. In conclusion, the dynamic stiffness at 400 Hz was selected as the best representative value to compare bituminous samples. In addition, the differences of dynamic stiffness at this frequency were considered related to tyre/road noise attenuations.

In the previous studies, (Merenda et al., 2019; Praticò et al., 2021b, 2021a) focused on the relationships between tyre/road noise and the frequency-based mechanics of pavements (e.g., pavement frequency response functions) in case of bituminous mixtures with the addition of crumb rubber (CR). For the mixes investigated, the conclusions were that an increase of percentage of CR (x-axis in Figure 2) and the corresponding variations in terms of air voids implied 1) the decrease of mechanical impedance (MI), 2) the decrease of the area under the impedance curve in 50-1250 Hz (Area MI), 3) the increase of the damping ratio (ζ), 4) the decrease of the modulus (E), 5) the decrease of the maximum acoustic response (maxAR) (see Figure 2). Y-axis represents the percentages as a function of the corresponding maximum (i.e., $E = E_i/\max E_i$).
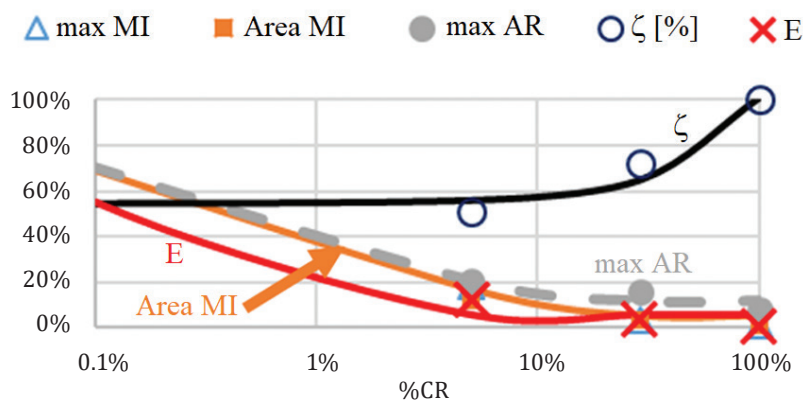
Figure 2. CR impact on noise (AR) and mechanistic response (MI, ζ, and E) elaborated from (Praticò et al., 2021b, 2021a)

Table 1. Use of FRF

In relation to	Description	Ref.
Moduli (E)	Determination of the complex modulus of the bone	(Gerdeen, 1975)
	Ultrasonic technique for measuring complex moduli of asphalt concrete	(van Velsor et al., 2011)
	A non-resonance, forced vibration technique for determining the complex dynamic stiffness of viscoelastic material	(Oyadiji & Tomlinson, 1994)
	Determination of the dynamic modulus of hot-mix asphalt (HMA) with a non-destructive impact resonance (IR) test	(Kweon & Kim, 2006)
	Determination of dynamic modulus of elasticity of concrete from the flexure fundamental resonant frequency	(Bede & Kožar, 2016)
	Determination of the dynamic and static Young modulus, and the dynamic stiffness of a cork agglomerate	(Policarpo et al., 2010)
	Determination of the dynamic modulus of asphalt concrete mixtures using a non-destructive test	(Mun, 2015)
Resonance (ω_n)	Mechanical Impedance of the human body in sitting and standing position at low frequencies	(Coermann, 1962)
	Use of mechanical impedance to follow changes in the paint-film rheology during drying and curing	(Strivens, 1999)
	Shift of primary resonance frequency relative to changes in the acceleration level	(Smith & Kazarian, 1994)
	Mechanical Impedance of a human body: the resonance frequency reduces when the vibration magnitude increases	(Griffin, 2001)
	Shift of resonant frequency and impact on damping	(Schubert et al., 2010)
Bio-mechanics	Determination of resistive and reactive components of the impedance of the human head and mastoid	(Corliss & Koidan, 1955)
	Determination of the degree of the union of healing femoral neck fractures by measurement of mechanical impedance	(Cambpell & Jurist, 1971)
	Dynamic characterization of a biological system by means of mechanical impedance techniques	(Suggs & Abrams, 1971)
	A mechanical impedance review and its relations with motor control, limb dynamics, and motion biomechanics	(Mizrahi, 2015)
Rolling noise	An in-situ method for mechanical impedance testing of soft surfaces	(Bendtsen et al., 2013)
	Use of mechanical impedance as the most relevant parameter in selecting a quieter mixture	(Morcillo et al., 2019)
	Dynamic stiffness of different bituminous mixtures assessed by means of the Non-Resonant Method	(Vázquez & Paje, 2015)
	Investigation of the relationships between road acoustic response and FRFs in case of bituminous mixtures	(Praticò et al., 2021b)
Structural health	Use of the impulse response method applied to concrete bridge decks	(Clem et al., 2013)
	A practical guide to carry out good FRF measurements	(Brown et al., 2015)
	Analysis of NDT technologies that can detect and characterize deterioration in bridge decks.	(Gucunski et al., 2013)
Crack detection	Use of impact tests to detect damage in reinforced concrete slabs	(Pimentel et al., 2017)
	Identification of the crack existence in shafts using the mechanical impedance approach	(Tlaisi et al., 2012)

Filippo G. Pratico,
Gianfranco Pellicano,
Matteo Bolognese,
Gaetano Licitra

A study
on frequency
response functions
in pavement
engineering

Unfortunately, despite the fact that FRFs are an engineering source of in-depth insights, too many methods are used for FRF assessment (as a function of the forced vibration type) and a quite high number of boundary conditions are given. Because so many methods are used to derive FRFs, it is difficult to compare different studies and discover the rationale behind them. Furthermore, this implies uncertainties and issues when focusing on the impact of waste materials and mixture composition.

1. Aims and tasks

The aims of the experimental investigation presented in this paper were i) to analyse the differences between the axial mechanical impedance (complex ratio of force and velocity taken at the same point) named *driving-point impedance* and the non-axial mechanical impedance (complex ratio of force at point *i* and velocity at point *j*), named *transfer impedance;* ii) to analyse the effects of crumb rubber (2% by mixture weight) and the percentage of bitumen (6.1% vs. 6.4% by mixture weight) on mechanical impedance in asphalt concrete specimens.

The study presented in this paper is structured so as to adress the following tasks (cf. Figure 3):

Task 1. Analysis of the boundary conditions, experimental set-up, and materials (Section 2).

Task 2. Time-domain analyses (Sections 1 and 3.2). Analysis of method fidelity and the relationships between the methods.

Task 3. Frequency-domain analyses (Sections 3.3, 3.4, 3.5). Analysis of the impact on the results of the method, CR percentage, and bitumen.

Task 4. Conclusions.

2. Method and materials

2.1. Boundary conditions

Sample excitation can be carried out using different methods and devices (e.g., exciters, hammers, and small balls) Under the hypothesis of using a hammer to excite the sample (and not an exciter), Figure 4 and Table 2 present the preliminary analysis of the main boundary conditions. Figure 4 illustrates the hierarchical tree of the main boundary conditions that can affect mechanical impedance, MI, including carrying out tests on pavement or samples, with different tips (rubber

tip, RT, and plastic tip, PT), from different heights (e.g., 4.5, 9, and 18 cm), focusing on the frequency domain, F, or on the time domain, T. In Table 2, cases A, B, D, and E refer to the *transfer impedance* (where acceleration and force are not measured on the same axis, nonaxial, NA), the remaining ones – to the *driving-point impedance* (where acceleration and force are measured along the same axis, coaxial, CA). Two different boundary conditions are considered (force and the type of the tip).

Indeed, the Mechanical Impedance can be determined considering different forces (based on the height and sample-hammer interaction), different types of hammer tips (e.g., plastic and rubber tip), and different positions of the accelerometer with respect to the hammer hit point. Overall, eight main combinations can be considered (see Table 2).
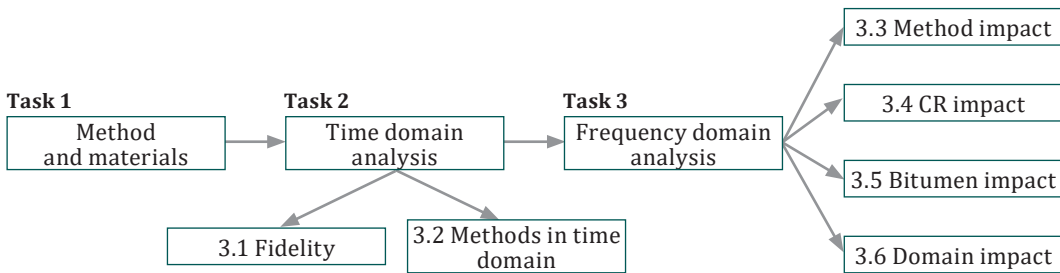
Figure 3. Main tasks
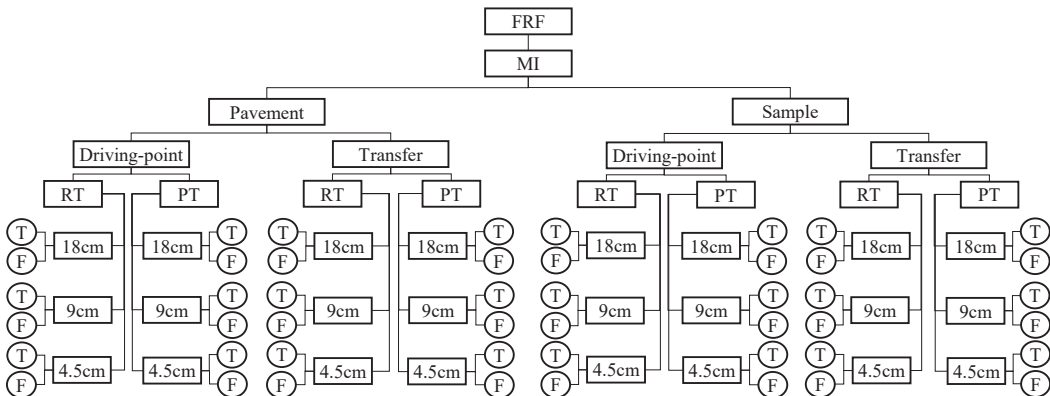
Symbols: FRF: Frequency Response Function; MI: Mechanical Impedance;
RT: Rubber Tip; PT: Plastic Tip; T: Time domain; F: Frequency domain;
CR: Crumb Rubber.

Figure 4. Hierarchical tree diagram of the main FRF boundary conditions

Filippo G. Pratico,
Gianfranco Pellicano,
Matteo Bolognese,
Gaetano Licitra

A study
on frequency
response functions
in pavement
engineering

Based on the results of preliminary analysis, in this study, four main schemes were selected (Methods 1 to 4), based on the type of hammer tip (plastic tip, PT, or rubber tip, RT), on meeting a condition of controlled force or controlled height of the hammer hit (controlled force, CF, or controlled height, CH), and on the position of the accelerometer with respect to the position of the hammer spot (i.e., coaxial, CA, or nonaxial, NA).

It is worth noting that in the CF condition, the force was about 20–25 N, while in the case of CH, the height was 18 cm. Based on the above, Figure 4 summarises the four selected methods to assess MI, namely:

Method 1 (PT, CH, NA) and *Method 2* (RT, CH, NA). In this case, the hammer (with the plastic tip for Method 1 and rubber tip for Method 2) hits the sample from a height of 18 cm. The load is measured through its load cell, while the acceleration is measured using the monoaxial accelerometer located at 2 cm from the hammer spot. This scheme (see Figure 5a) represents Method 1 and Method 2 and is used to calculate the *transfer impedance*.

Method 3 (RT, CF, CA). In this case, the hammer (with the rubber tip) hits the impedance head located over the sample from a variable height (with respect to the sample) in order to obtain a force of about 20–25 N. Note that the sensitivity of the convert charge transducer is 1 mV/pC, where mV stands for millivolt and pC – for pico Coulomb. A force greater than 25 N would generate an overload due to an excess force applied to the impedance head. The load applied and the acceleration are measured through the same impedance head. This scheme represents Method 3 and is used to derive the *driving point impedance* (see Figure 5b). Impedance heads are widely used. Notwithstanding, the introduction of this "supplementary" mass can

Table 2. Preliminary analysis of boundary conditions

Method1	Method2	Method3	Method4	Method5	Method6	Method7	Method8	Parameter
CH	CH	CF	CF	CF	CF	CH	CH	Controlled Height, CH, or Controlled Force, CF
PT	RT	RT	RT	PT	PT	PT	RT	Rubber Tip, RT, or Plastic Tip, PT
NA	NA	CA	NA	NA	CA	CA	CA	Nonaxial, NA, or Coaxial, CA
A	B	C	D	E	F	G	H	

Symbols: CH: Controlled Height; CF: Controlled Force; PT: Plastic Tip;
    RT: Rubber Tip; NA: Nonaxial; CA: Coaxial

lead to differences between the force applied to the structure and the force sensed by the impedance head (force trasducer, cf. (Buzdugan et al., 1986)).

Method 4 (RT, CF, NA). In this case, the hammer (with the rubber tip) hits the impedance head (located over the sample) from a variable height (with respect to the sample) in order to obtain a force of about 20–25 N. The load applied is measured through the impedance head while the acceleration is measured using the monoaxial accelerometer located at 2 cm from the impedance head. This scheme represents Method 4 and is used to calculate the *transfer impedance* (see Figure 5c).
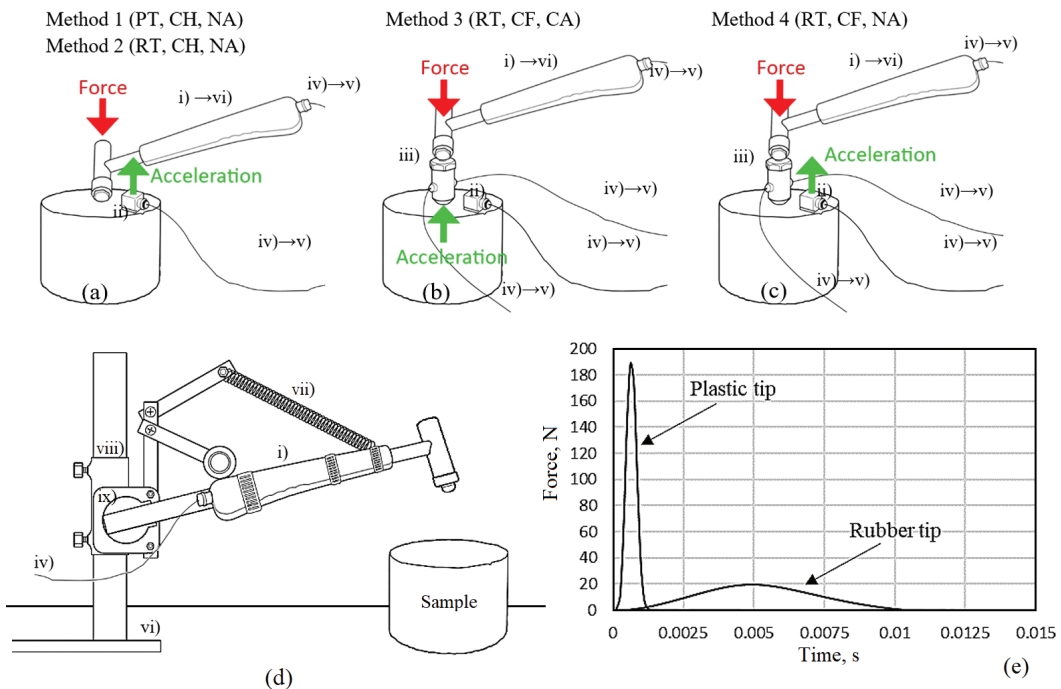
Note. i) hammer; ii) accelerometer; iii) impedance head; iv) acquisition board; v) laptop: vi) height control device; vii) spring; viii) sliding part that allows changing the height; ix) rotating hinge. PT: Plastic Tip. RT: Rubber Tip. CH: Controlled Height. CF: Controlled Force. CA: Coaxial. NA: Nonaxial. The drop height was referred to the vertical distance between the hammer tip and sample surface (for Methods 1 and 2) or impedance head surface (for Methods 3 and 4)

Figure 5. Test set up. (a) Method 1/Method 2, (b) Method 3, (c) Method 4, (d) device to control the reference height of the hammer, (e) impulse shape of force as function of the hammer tip

Filippo G. Pratico,
Gianfranco Pellicano,
Matteo Bolognese,
Gaetano Licitra

A study
on frequency
response functions
in pavement
engineering

2.2. Experimental set up

To pursue the objectives set above and to analyse the differences between the axial mechanical impedance (complex ratio of force and velocity taken at the same point, *the driving-point impedance*) and the non-axial mechanical impedance (complex ratio of force at point *i* and velocity at the point *j, transfer impedance*), the following hardware was used (cf. Figure 1 (IR) and Figure 5):

An impact hammer 'Bruel & Kjaer Type 8206' to register the applied force for the *transfer impedance*. The output sensitivity is expressed in terms of voltage per unit force (mV/N or mV/lbf). The hammer features an acceleration compensation that removes the unwanted noise generated by the resonance of the hammer from the output signal. This results in a clean and smooth output signal, representing the excitation in both amplitude and phase. The hammer is supplied with a set of three interchangeable impact tips made from aluminium, plastic (Delrin), and rubber (Polyurethane): the choice of the kind of tip affects the amplitude and duration of the impulse shape (Bruel & Kjaer, 2018). Figure 5e illustrates an example of impulse shape in the case of sample UGE PCR2 for Method 1 (plastic tip) and Method 4 (rubber tip);

A piezoelectric accelerometer 'Bruel & Kjaer Type 4507' with a frequency range of 0.3–6000 Hz to measure and register the acceleration for the *transfer impedance*;

An impedance head 'Bruel & Kjaer Type 8001'to measure and register the *driving-point impedance*;

A Bruel & Kjaer front-end acquisition board used to convert the hammer and impedance head's time series to frequency responses using the Fast Fourier Transform (FFT);

A laptop computer to acquire signals;

A pivot-based device to control the reference height (cf. Figure 5d). This latter was set up based on the first prototype jointly set up in 2019 at iPOOL s.r.l., a spin-off of the Italian National Research Center (Pisa, Italy).

2.3. Materials

In order to pursue the objectives mentioned above, asphalt concretes with the same nominal maximum aggregate size (6 mm) with or without crumb rubber were made and tested. It is worth noting noting that (cf. Tables 3 and 4): i) the specimens AC6o_55, AC6o_56, AC6o_59, and AC6o_60 were produced using a gyratory compactor 'Rainhart' (EN 12697-31:2019). The crumb rubber was incorporated

Table 3. Main characteristics of the tested samples

		B, %	CR, %	Number of revolutions of the gyratory compactor	Sample diameter, mm	G_{mbDIM}	Alternative terminology	
1	AC6o_55	6.1	2(*)	130	97.5	2.393	1_2%CR_6.1%B	Lab produced
2	AC6o_56	6.4	2(*)	130	97.5	2.385	2_2%CR_6.4%B	Lab produced
3	AC6o_59	6.1	2(**)	130	97.5	2.292	3_2%UCR_6.1%B	Lab produced
4	AC6o_60	6.4	2(**)	130	97.5	2.204	4_2%UCR_6.4%B	Lab produced
5	UGE P1	6.4	0	On-site compaction	98.9	2.115	5_0%CR_6.4%B	Core
6	UGE PCR1	6.4	2	On-site compaction	99.0	2.019	6_2%CR_6.4%B	Core
7	UGE P2	6.4	0	On-site compaction	99.0	2.131	7_0%CR_6.4%B	Core
8	UGE PCR2	6.4	2	On-site compaction	99.3	2.030	8_2%CR_6.4%B	Core

Symbols: AC6: Asphalt concrete with nominal maximum aggregate size of 6 mm;
B: Bitumen by mixture weight; CR: Crumb rubber by mixture weight;
$G_{mb\,DIM}$: Bulk specific gravity calculated considering the dimensions
and weight of the sample.
(*) RARX
(**) Untreated Crumb Rubber (UCR)
Note: An alternative terminology is reported to simplify the identification
of samples tested.
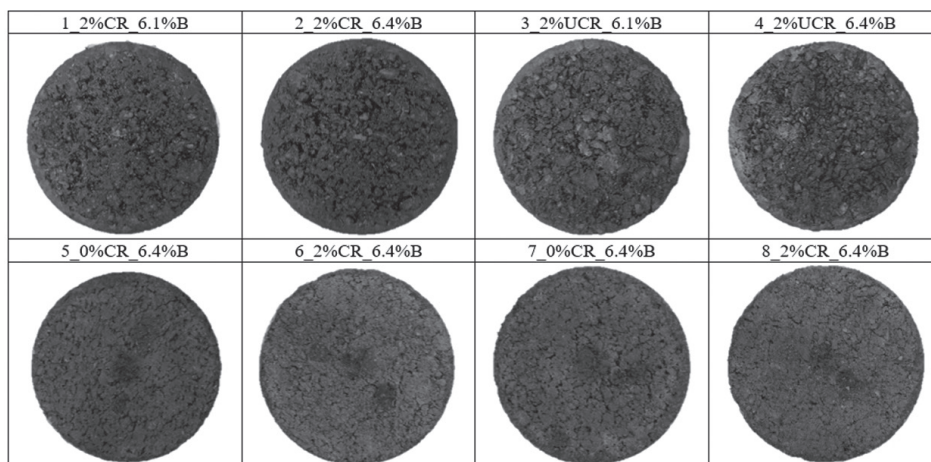
Figure 6. Upper surface of the tested samples

Filippo G. Pratico,
Gianfranco Pellicano,
Matteo Bolognese,
Gaetano Licitra

A study
on frequency
response functions
in pavement
engineering

into the mixtures adopting the dry process: for specimens AC6o_55 and AC6o_56, RARX was used while for AC6o_59 and AC6o_60 untreated crumb rubber (UCR) was used. ii) Samples UGE P1, UGE PCR1, UGE P2, and UGE PCR2 were extracted from a pavement by coring.

Table 4. Main scheduled tests and standards

Test	Parameter	Unit of measure	Standard	Ref.
Dimensional analysis	Diameter (D)	mm	UNI EN 12697-36	(EN 12697-36, 2006)
	$G_{mb\ COR}$	dimensionless	ASTM D6752 / D6752M ASTM D6857 / D6857M	(Griffin, 2001; Strivens, 1999; Suggs & Abrams, 1971)
	AV_{COR}	%		
	$G_{mb\ DIM}$	dimensionless		
	Voids Mineral Aggregate (VMA)	dimensionless	AASHTO M323	(AASHTO M 323, 2017)
	Voids Filled Asphalt (VFA)	dimensionless		
Macro-texture	Mean texture depth (MTD)	mm	UNI EN 13036-1 ASTM E965-15	(ASTM E965-15, 2019; EN 13036-1, 2010)
Mechanical response	Mechanical Impedance (MI)	N·s/m	UNI EN 29052-1	(EN 29052-1, 1992; Praticò, 2007; Praticò et al., 2021b)

Table 5. Results for volumetric tests and macro-texture

	1_2%CR_6.1%B	2_2%CR_6.4%B	3_2%UCR_6.1%B	4_2%UCR_6.4%B	5_0%CR_6.4%B	6_2%CR_6.4%B	7_0%CR_6.4%B	8_2%CR_6.4%B
Diameter	97.5	97.5	97.5	97.5	98.9	99.0	99.0	99.3
$G_{mb\ COR}$	2.399	2.376	2.311	2.267	2.119	2.051	2.130	2.092
AV_{COR}	1.28	2.21	4.91	6.70	11.80	13.09	11.30	11.37
MTD	0.560	0.561	0.784	0.884	0.322	0.277	0.299	0.207

Symbols: CR: Crumb Rubber; UCR: Untreated Crumb Rubber; B: Bitumen;
$G_{mb\ COR}$: ulk specific gravity measured using the Corelok machine;
AV_{COR}: Air void content measured using the Corelok machine

Table 6. Average, standard deviation and repeatability of F_{max}, A_{max}, V_{max}, D_{max} and F_{max}/V_{max}.

Symbols: F_{max}: max force; A_{max}: max acceleration; V_{max}: max velocity; D_{max}: max deflection; M: average; St.dev.s: sample standard deviation; r: repeatability. N.B. Time-based values

	Height, cm	F_{max}, N				A_{max}, m/s²				V_{max}, m/s			
		M	St.dev.s	r	r/M	M	St.dev.s	r	r/M	M	St.dev.s	r	r/M
Method1	18	198.2	15.7	43.5	0.2	1.1E+02	3.1E+01	85.9	0.8	5.1E-03	9.7E-04	2.7E-03	0.5
Method1	9	87.7	8.1	22.5	0.3	2.5E+01	8.3E+00	23.0	0.9	2.1E-03	2.9E-04	8.0E-04	0.4
Method1	4.5	14.7	1.9	5.3	0.4	2.5E+00	7.6E-01	2.1	0.8	1.1E-03	1.7E-04	4.7E-04	0.4
Method2	18	34.2	2.3	6.4	0.2	3.6E-01	3.1E-02	0.1	0.2	4.0E-04	4.7E-05	1.3E-04	0.3
Method2	9	19.8	0.5	1.4	0.1	1.9E-01	2.4E-02	0.1	0.4	2.2E-04	3.6E-05	1.0E-04	0.5
Method2	4.5	4.8	0.3	0.8	0.2	5.0E-02	1.2E-02	0.03	0.7	7.6E-05	4.9E-05	1.4E-04	1.8
Method3	18	20	0.6	1.7	0.1	4.3E+00	1.9E-01	0.5	0.1	1.0E-02	5.8E-04	1.6E-03	0.2
Method3	9	11.6	0.8	2.2	0.2	3.0E+00	6.3E-01	1.7	0.6	6.5E-03	5.7E-04	1.6E-03	0.2
Method3	4.5	5.8	0.6	1.7	0.3	1.5E+00	3.4E-01	0.9	0.6	3.7E-03	7.4E-04	2.1E-03	0.6
Method4	18	20	0.6	1.7	0.1	3.6E+00	4.5E-01	1.2	0.3	2.2E-03	2.3E-04	6.4E-04	0.3
Method4	9	11.6	0.8	2.2	0.2	2.2E+00	5.9E-01	1.6	0.7	1.5E-03	3.0E-04	8.3E-04	0.6
Method4	4.5	5.8	0.6	1.7	0.3	5.7E-01	1.5E-01	0.4	0.7	3.2E-04	9.5E-05	2.6E-04	0.8

	Height, cm	D_{max}, m				F_{max}/V_{max}, N s/m			
		M	St.dev.s	r	r/M	M	St.dev.s	r	r/M
Method1	18	4.5E-06	2.6E-07	7.2E-07	0.2	3.9E+04	1.6E+04	4.4E+04	1.1
Method1	9	3.0E-06	3.7E-07	1.0E-06	0.3	4.2E+04	2.8E+04	7.8E+04	1.8
Method1	4.5	1.8E-06	3.2E-07	8.9E-07	0.5	1.3E+04	1.1E+04	3.0E+04	2.3
Method2	18	1.8E-06	1.8E-07	5.0E-07	0.3	8.5E+04	4.9E+04	1.4E+05	1.6
Method2	9	1.1E-06	1.2E-07	3.3E-07	0.3	9.2E+04	1.3E+04	3.6E+04	0.4
Method2	4.5	4.1E-07	3.5E-07	9.7E-07	2.4	6.3E+04	7.1E+03	2.0E+04	0.3
Method3	18	2.6E-06	5.1E-07	1.4E-06	0.5	2.0E+03	1.1E+03	3.0E+03	1.5
Method3	9	1.3E-06	4.8E-07	1.3E-06	1.0	1.8E+03	1.4E+03	3.9E+03	2.2
Method3	4.5	7.3E-07	5.5E-07	1.5E-06	2.1	1.6E+03	7.6E+02	2.1E+03	1.3
Method4	18	1.4E-06	1.8E-07	5.0E-07	0.4	9.0E+03	2.7E+03	7.5E+03	0.8
Method4	9	1.0E-06	4.9E-07	1.4E-06	1.4	7.9E+03	2.6E+03	7.2E+03	0.9
Method4	4.5	6.1E-07	5.6E-07	1.6E-06	2.5	1.8E+04	5.9E+03	1.6E+04	0.9

Filippo G. Pratico,
Gianfranco Pellicano,
Matteo Bolognese,
Gaetano Licitra

A study
on frequency
response functions
in pavement
engineering

UGE mixtures are based on the same formulation. UGE P1 and UGE P2 do not contain crumb rubber, while UGE PCR1 and UGE PCR2 contain crumb rubber, CR (2% by mix weight). In Table 3, the main features (such as the percentage of bitumen and crumb rubber, dimensional and volumetrics characteristics) are described, while Figure 6 illustrates the upper surfaces of the tested samples.

To this end, it is noteworthy that Samples 1–4 yield an MTD-AV relationship where macrotexture increases along with air void content. In contrast for Samples 5–9 (on-site compaction), the macrotexture appears lower and its relationship with AV is quite negligible.

Focusing on volumetric and mechanical properties, several laboratory tests were carried out. In particular, tests were performed for: 1) dimensional analysis, 2) bulk specific gravity, 3) sand patch, 4) mechanical impedance and dynamic stiffness. Table 4 gives an overview of the main scheduled tests and the standards followed. Table 5 provides the summary of the results.

3. Results

3.1. Precision of the methods

As it is widely known, precision may refer to repeatability or reproducibility conditions. In turn, the latter are the factors that impact uncertainty. This section refers to the analysis carried out to assess the precision of each method. In Table 6, the values of average, M, standard deviation (St.dev.s, sample standard deviation), and repeatability, r (Ferrari & Giannini, 2000; ISO 5725-1, 1994) of F_{max} (max force), A_{max} (max acceleration), V_{max} (max velocity), D_{max} (max deflection) and F_{max}/V_{max} (ratio between max force and max velocity) are reported. For each method, 31 hits were applied and three different heights of the hammer were considered (18, 9, and 4.5 cm). To assess precision, the tests were carried out on a single specimen ('AC6o_60', 6.4% of bitumen and 2% of untreated crumb rubber). After each test, the accelerometer was removed and then replaced.

Figure 7 illustrates how height and test method affect results. Figure 8 illustrates the results obtained in terms of repeatability (r) (or single-operator precision or d2s, c.f. ASTM C670, ASTM E177, and ISO 5725-1) and in terms of corresponding r/M ratio (or difference two-sigma limit in percent, d2s%). It should be noted that despite the differences in terms of M and r, r/M appears to be less variable than r (cf. Table 6). Even if a limited number of points were provided in each curve due to the time-consuming tests and the scheduled plan of experiments,
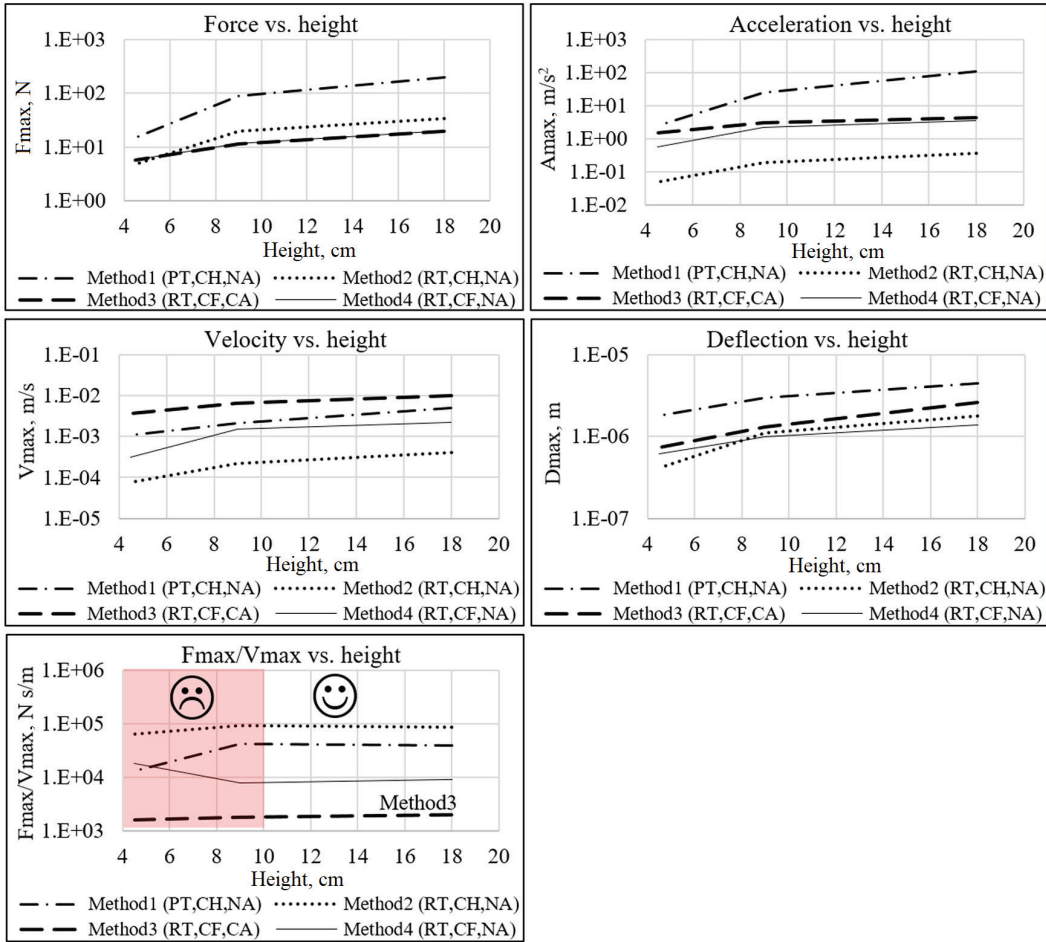
Figure 7. Comparison of Mechanical Impedance considering the four methods used (time-based values)
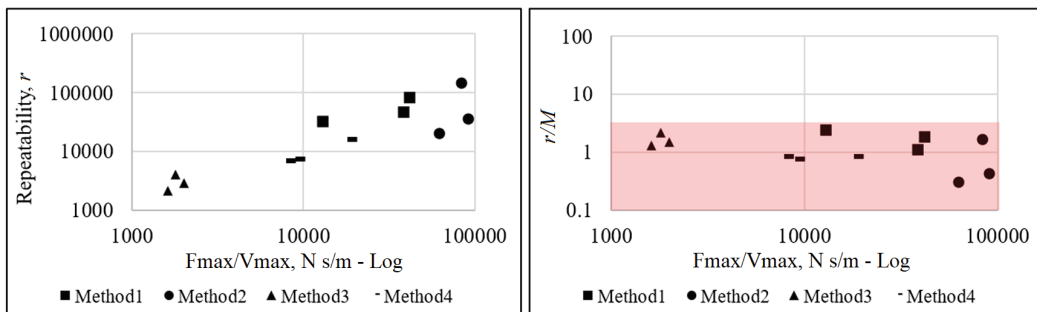
Figure 8. Repeatability and r/M of F_{max}/V_{max}

Filippo G. Pratico,
Gianfranco Pellicano,
Matteo Bolognese,
Gaetano Licitra

A study
on frequency
response functions
in pavement
engineering

under the precision conditions specified above, Figures 7 and 8 seem to point out that while r depends on height (e.g., for F), r/M appears quite constant. While repeatability r is very high, r/M variability appears somehow lower and it ranges from 0.1 to 2.5. Multiplying by 4 the height (cf. Table 7), F_{max} increases, A_{max} increases, as well as V_{max}, D_{max}, and F_{max}/V_{max}. r and r/M are both quite high but, importantly, r/M appears to be reasonably independent on test conditions and results. Importantly, heights higher than 10 cm seem to lead to results that do not depend on height. In summary, signals over time, namely F/V, are less dependent on h when $h > 10$ cm and precision statements should be based on coefficients of variation (r/M instead of r).

Table 7. Impact of height on F_{max}, A_{max}, V_{max}, D_{max} and F_{max}/V_{max} (time-based analysis)

Parameter	F_{max}				A_{max}				V_{max}				D_{max}				F_{max}/V_{max}			
Method	1	2	3	4	1	2	3	4	1	2	3	4	1	2	3	4	1	2	3	4
Height Impact*	13	7	3.5	3.5	44	7	3	6.3	4.6	5.3	2.7	7	2.5	4.4	3.5	2.3	3.2	1.4	1.2	2.3

*Impact on the given parameter when height is multiplied by 4

3.2. Correlation between methods in the time domain

Table 8 focuses on how different parameters (e.g., F_{max}) in time domain depend on the method for different samples. Three replicates per test were carried out. The average values of F_{max}, N, A_{max}, m/s², V_{max}, m/s, D_{max}, m and the ratio F_{max}/V_{max}, N·s/m are summarised.

Table 8. F_{max}, A_{max}, V_{max}, D_{max} and F_{max}/V_{max} of the tested samples (time-based values)

	F_{max}, N				A_{max}, m/s² · 10				V_{max}, m/s · 10⁴			
Method	1	2	3	4	1	1	3	4	1	2	3	4
Max	254	40	22	22	1600	8	65	6	140	10	210	20
Min	189	33	17	17	480	2	26	1	39	2	90	2
Average	225	36	19	19	1046	4	37	2	80	5	124	5

	D_{max}, m · 10⁷				F_{max}/V_{max}, N·s/m · 10⁻³			
Method	1	2	3	4	1	1	3	4
Max	87	37	530	13	55	140	2	130
Min	22	11	19	9	14	38	1	8
Average	35	17	93	8	34	95	2	76

Table 9 refers to signals over time and points out that force with Method 1 is the highest, such as acceleration and velocity, while the ratio Fmax/Vmax with Method 2 is the highest.

Considering Method 3 (where the hammer hits on the impedance head) as the reference, in order to derive the driving-point impedance, the following conclusions can be drawn:

1. The force obtained with Method 3 is about 0.09 times the force obtained with Method 1, 0.53 times the force obtained with Method 2 and the same used for Method 4;

Table 9. Main statistics of signals over time

	F_{max}, N			
	Method1	Method2	Method3	Method4
Max	$F_{max3} \cdot 11.55$	$F_{max3} \cdot 1.82$	F_{max3}	F_{max3}
Min	$F_{max3} \cdot 11.12$	$F_{max3} \cdot 1.94$	F_{max3}	F_{max3}
Average	$F_{max3} \cdot 11.70$	$F_{max3} \cdot 1.89$	F_{max3}	F_{max3}

	A_{max}, m/s^2			
	Method1	Method2	Method3	Method4
Max	$A_{max3} \cdot 24.62$	$A_{max3} \cdot 0.12$	A_{max3}	$A_{max3} \cdot 0.10$
Min	$A_{max3} \cdot 18.46$	$A_{max3} \cdot 0.07$	A_{max3}	$A_{max3} \cdot 0.04$
Average	$A_{max3} \cdot 28.37$	$A_{max3} \cdot 0.11$	A_{max3}	$A_{max3} \cdot 0.07$

	V_{max}, m/s			
	Method1	Method2	Method3	Method4
Max	$V_{max3} \cdot 0.67$	$V_{max3} \cdot 0.05$	V_{max3}	$V_{max3} \cdot 0.10$
Min	$V_{max3} \cdot 0.43$	$V_{max3} \cdot 0.03$	V_{max3}	$V_{max3} \cdot 0.02$
Average	$V_{max3} \cdot 0.65$	$V_{max3} \cdot 0.04$	V_{max3}	$V_{max3} \cdot 0.04$

	F_{max}/V_{max}, N·s/m			
	Method1	Method2	Method3	Method4
Max	$F_{max3}/V_{max3} \cdot 30.56$	$F_{max3}/V_{max3} \cdot 77.78$	F_{max3}/V_{max3}	$F_{max3}/V_{max3} \cdot 72.22$
Min	$F_{max3}/V_{max3} \cdot 14.00$	$F_{max3}/V_{max3} \cdot 38.22$	F_{max3}/V_{max3}	$F_{max3}/V_{max3} \cdot 8.10$
Average	$F_{max3}/V_{max3} \cdot 20.62$	$F_{max3}/V_{max3} \cdot 58.15$	F_{max3}/V_{max3}	$F_{max3}/V_{max3} \cdot 46.93$

Filippo G. Pratico,
Gianfranco Pellicano,
Matteo Bolognese,
Gaetano Licitra

A study
on frequency
response functions
in pavement
engineering

2. The acceleration obtained with Method 3 is about 0.04 times the acceleration obtained with Method 1, 9.34 times the acceleration obtained with Method 2 and 15.05 times the acceleration obtained with Method 4;
3. The velocity obtained with Method 3 is about 1.55 times the velocity obtained with Method 1, 26.19 times the velocity obtained with Method 2 and 23.29 times the velocity obtained with Method 4;
4. The F_{max}/V_{max} ratio obtained with Method 3 is about 0.05 times the F_{max}/V_{max} ratio obtained with Method 1, 0.02 times the F_{max}/V_{max} ratio obtained with Method 2 and 0.02 times the F_{max}/V_{max} ratio obtained with Method 4.

In Table 9, the correlation between F_{max}, A_{max}, V_{max}, and F_{max}/V_{max} obtained with Method 3 and the other methods is reported for each tested sample.

It can be summarized that the four methods give MIs that are very different, except that for Methods 2 and 4:

$F_{max3} = 0.1 \cdot F_{max1} = 0.5 \cdot F_{max2} = F_{max4}$
$A_{max3} = 0.03 \cdot A_{max1} = 9.3 \cdot A_{max2} = 18.5 \cdot A_{max4}$
$V_{max3} = 1.4 \cdot V_{max1} = 23.8 \cdot V_{max2} = 24.8 \cdot V_{max4}$
$A_{max3} / F_{max3} = 0.3 \cdot A_{max1} / F_{max1} = 18.6 \cdot A_{max2} / F_{max2} = 18.5 \cdot A_{max4} / F_{max4}$
$F_{max3} / V_{max3} = 0.1 \cdot F_{max1} / V_{max1} = 0.02 \cdot F_{max2} / V_{max2} = 0.02 \cdot F_{max4} / V_{max4}$

3.3. Correlation between methods in the frequency domain

A recurrent issue in data interpretation is that sometimes the *driving-point* strategy is used (Vázquez & Paje, 2015) instead of the *transfer impedance* (Li et al., 2016) or *vice versa.*

When it comes to the frequency domain, Table 10 refers to the averages of MI for frequencies lower than 3.2 kHz. Here, the difference between the *driving-point impedance* (Method 3) and the *transfer impedance* (average of Methods 1, 2 and 4) is reported.

Figure 9 illustrates the results obtained in terms of Mechanical Impedance (MI) as a function of frequency according to Methods 1 to 4, testing the samples depicted in Figure 6. Overall, MI3 is the lowest, while the remaining MIs (i.e., 1, 2, 4) appear to be higher and partly overlapping. With respect to the *driving-point impedance* (Method 3), using Methods 1, 2, and 4, a minimum reduction of 13 dB (in the case of 3_2%UCR_6.1%B) and a maximum reduction of 19 dB (in the case of 4_2%UCR_6.4%B) are observed. This can be explained as a consequence of a large damping of vibrations between the hammer hitting point (on

the impedance head) and the accelerometer (located at about 2 cm). In Table 11, the Pearson coefficients between the Mechanical Impedance with the four Methods and air void (AV_{COR}), bulk specific gravity ($G_{mb\,COR}$ and $G_{mb\,DIM}$) and mean texture depth (MTD) are presented. In Table 12, the values of the driving-point impedance and those of the transfer impedance as reported in the literature and observed in this study (UNIRC) are reported, in case of samples or pavements tested ($MI_{PAV} > MI_{SAMPLE}$).

It has been noted that:

1. When considering the average MI in 0–3.2 kHz, on average, *transfer impedance* is higher than *driving-point impedance* (cf. Table 10). This complies with the damping of vibration with distance, which implies lower speeds and higher MIs. It has been acknowledged that further insights could emerge in terms of modal analysis.

2. For Method 2 and Method 4, the Pearson coefficients (MI versus AV_{COR}) appear to be quite consistent with those repoerted in the literature (cf. Table 11).

3. Whatever the method (*driving-point impedance* or *transfer impedance)*, on average, MIs on pavements seem to be higher than the ones on samples. This complies with the dependence of deflection and speeds on the Poisson ratio (cf. Table 12). It is worth noting that in Table 12, UNIRC refers to this study.

Table 10. Difference (in dB, re 1 N·s/m) between *driving-point* and *transfer impedance* (frequency-based comparisons)

Sample	Driving-point impedance (average, dB) Method 3	Transfer impedance (average, dB) Methods 1–2–4	Difference, dB
1_2%CR_6.1%B	59	76	18
2_2%CR_6.4%B	62	78	16
3_2%UCR_6.1%B	61	74	13
4_2%UCR_6.4%B	56	75	19
5_0%CR_6.4%B	60	76	17
6_2%CR_6.4%B	60	74	15
7_0%CR_6.4%B	62	77	15
8_2%CR_6.4%B	60	74	14

*Filippo G. Pratico,
Gianfranco Pellicano,
Matteo Bolognese,
Gaetano Licitra*

A study
on frequency
response functions
in pavement
engineering
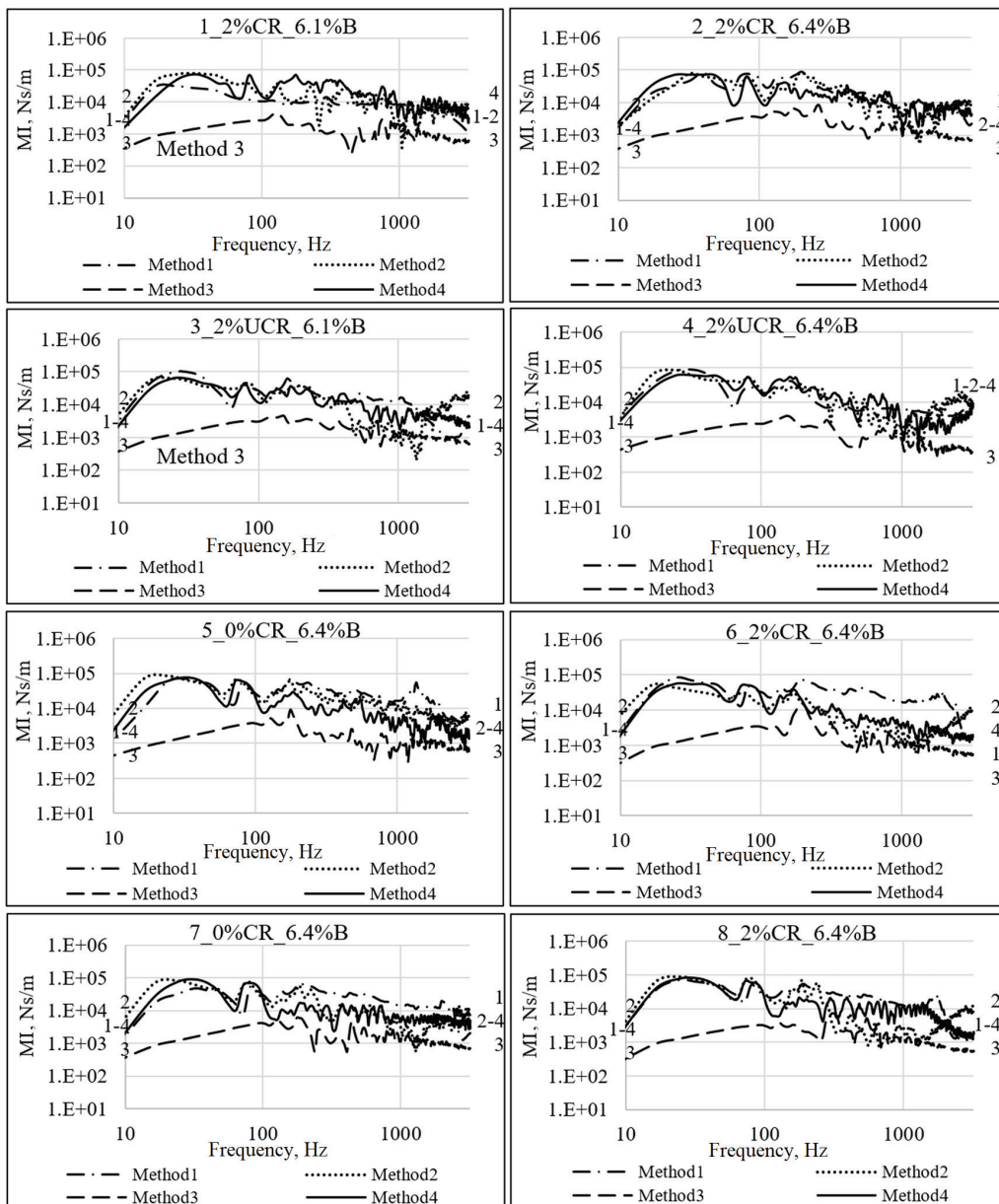
Figure 9. Comparison of Mechanical Impedance considering the four methods used

Table 11. Pearson coefficients

	MI1	MI2	MI3	MI4
AV_{COR}	0.68	−0.51	−0.01	−0.79
$G_{mb\ COR}$	−0.68	0.58	−0.01	0.77
$G_{mb\ DIM}$	−0.58	0.63	0.11	0.79
MTD	−0.68	0.45	−0.41	0.24

Symbols: MI1: Mechanical Impedance with Method 1; AV_{COR}: Air void content measured using the Corelok machine; $G_{mb\ COR}$: Bulk specific gravity measured using the Corelok machine; $G_{mb\ DIM}$: Bulk specific gravity calculated considering the dimensions and weight of the sample; MTD = Mean Texture Depth.

Table 12. Driving-point impedance and transfer impedance values

Driving-point (Average, dB)	ref.	Driving-point (Average, dB)	ref.		Driving-point (Average, dB)	ref.	Driving-point (Average, dB)	ref.
Sample		Pavement			Sample		Pavement	
Min				Min	27	(d)		
48	(a)							
48	(b)							
		54	(a)					
56	UNIRC							
62	(b)							
62	UNIRC							
					74	UNIRC		
		75	(c)					
					78	UNIRC		
					80	(a)		
					93	(e)		
							94	(a)
Max				Max	100	(e)		

Note: a – (Bendtsen et al., 2013); b – (Skov et al., 2015); c – (Morcillo et al., 2019); d – (Li et al., 2012); e – (Radenberg et al., 2017). UNIRC: max and min value obtained in this study

Filippo G. Pratico,
Gianfranco Pellicano,
Matteo Bolognese,
Gaetano Licitra

A study
on frequency
response functions
in pavement
engineering

3.4.   Effect of CR percentage

The use of recycled crumb rubber in asphalt pavements is gaining momentum due to possible environmental, structural, and acoustic benefits.

Figure 10 addresses the effect of the percentage of crumb rubber for different methods, where dotted curves correspond to mixtures with crumb rubber and solid curves to mixtures without crumb rubber.
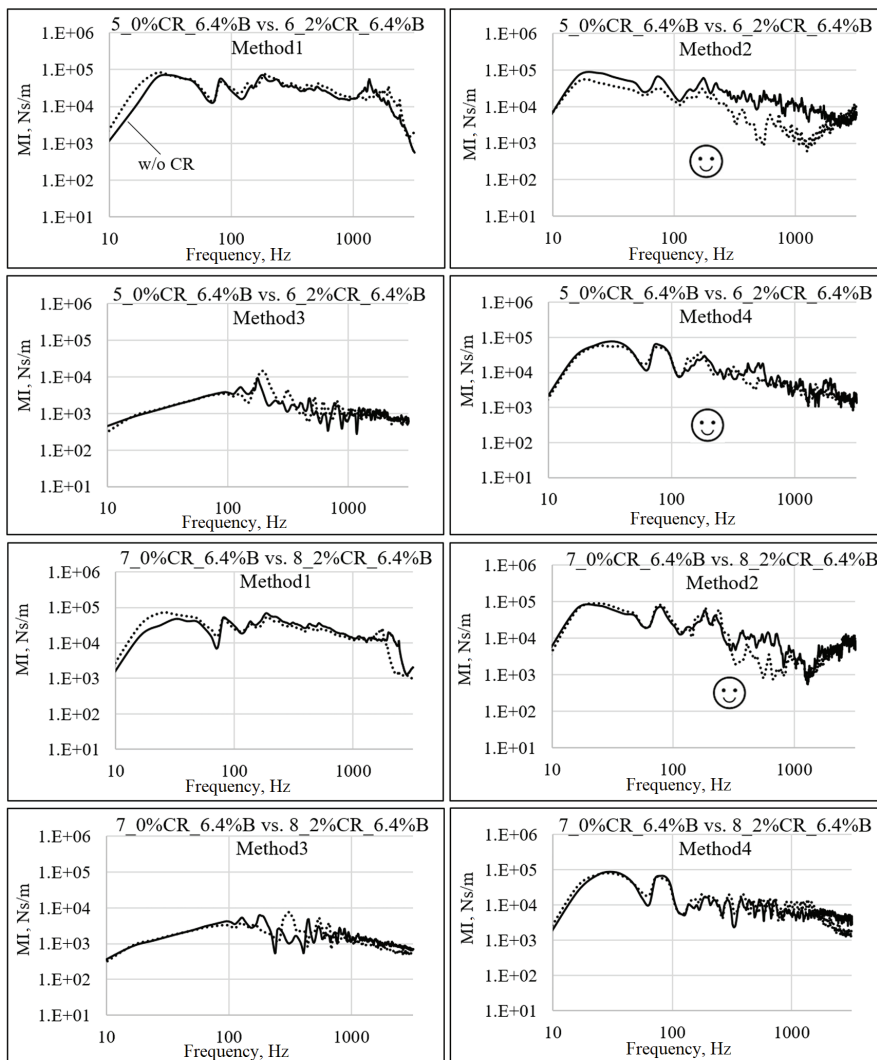
Figure 10. Comparison of Mechanical Impedance between 0%CR and 2%CR considering the four methods used

Even if uncertainties are given, for frequencies in 0.1–1 kHz, usually the mechanical impedance of the mixtures with crumb rubber is lower than that of the mixtures without crumb rubber (cf. also (Praticò et al., 2021c)).

Importantly, Method 2 (*transfer impedance*, rubber tip) better highlights the effect of adding crumb rubber on MI for frequencies in 0.1–1 kHz. This could depend on the impact of crumb rubber on the propagation and, consequently, on speeds.

3.5. Effect of bitumen percentage

Figure 11 deals with the effect of bitumen percentage, where higher bitumen percentages correspond to dotted curves.

It should be noted that, except for Method 4, in 0.1–1 kHz, the higher the bitumen percentage is, the higher the MI curve results. To this end, it has been noted that while Methods 1–2 for quasi-static conditions (low frequencies) seem to comply with the inverse proportionality between bitumen content and modulus (at least for percentages higher than the optimal ones, cf. (Alani et al., 2010; Shell International Petroleum
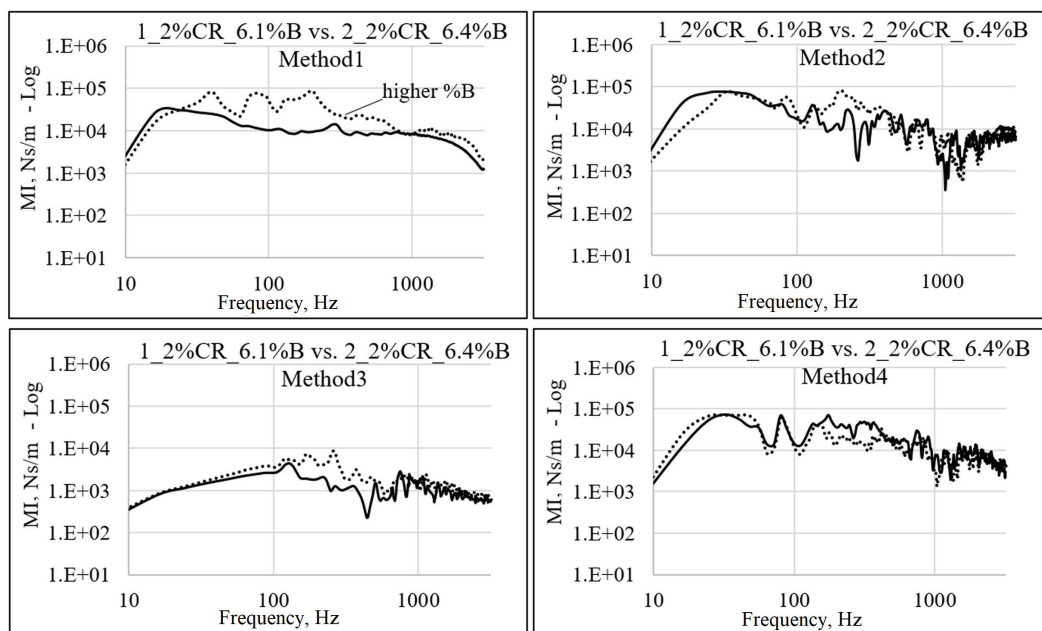
Figure 11. Comparison of Mechanical Impedance between 6.1% and 6.4% of bitumen considering the four methods used

Filippo G. Pratico,
Gianfranco Pellicano,
Matteo Bolognese,
Gaetano Licitra
A study
on frequency
response functions
in pavement
engineering

Company Limited, 1978)), this does not hold for Methods 3–4. This fact calls for further research considering higher percentages of bitumen.

In Table 13, the damping ratio of the samples obtained using the four methods is reported. The steps followed to derive the damping ratio are described in a previous study by the authors (Praticò et al., 2021b). On average, values range from 0.07 to 0.13 (which partly complies with (Hamet & Klein, 2004; Praticò et al., 2021b; Praticò & Vaiana, 2012)). CR-added mixtures have a damping ratio that is 6%–49% higher than the ones without crumb rubber. Importantly, for Method 2 (low acceleration, propagation path, and therefore signal attenuation) the highest increase of damping ratio is obtained (49% with respect to samples without crumb rubber).

This seems to strengthen the concept of proportionality between CR percentage and vibration mitigation. Finally, it has been noted that such an appreciable increase in the damping ratio with CR could strengthen the importance of CR for rolling noise (de León et al., 2020; Praticò et al., 2021b) and for bridge vibration control, particularly for timber bridges and other types of infrastructure for sustainable mobility, where

Table 13. Damping ratio derived using different methods

ζ	Method 1 (PT, CH, NA)	Method 2 (RT, CH, NA)	Method 3 (RT, CF, CA)	Method 4 (RT, CF, NA)	Max	Min	Average
1_2%CR_ 6.1%B	0.125	0.090	0.091	0.074	0.125	0.074	0.095
2_2%CR_ 6.4%B	0.077	0.075	0.075	0.081	0.081	0.075	0.077
3_2%UCR_ 6.1%B	0.090	0.069	0.073	0.081	0.090	0.069	0.078
4_2%UCR_ 6.4%B	0.077	0.074	0.112	0.080	0.112	0.074	0.086
5_0%CR_ 6.4%B	0.082	0.079	0.076	0.071	0.082	0.071	0.077
6_2%CR_ 6.4%B	0.097	0.088	0.093	0.073	0.097	0.073	0.087
7_0%CR_ 6.4%B	0.078	0.075	0.088	0.077	0.088	0.075	0.079
8_2%CR_ 6.4%B	0.102	0.088	0.105	0.085	0.105	0.085	0.095

Symbols: ζ: damping ratio; PT: Plastic Tip; RT: Rubber Tip; CH: Controlled Height; CF: Controlled Force; NA: nonaxial; CA: coaxial; CR: Crumb Rubber; UCR: Untreated Crumb Rubber; B: Bitumen.

vibration serviceability is the main design criterion (Bocci & Prosperi, 2020; Praticò & Vaiana, 2012; Schubert et al., 2010).

Even if further research and more data are needed, Methods 1 and 2, where the impedance head is not used and propagation path is involved, seem to better comply with two outstanding criteria: 1) lower MI for quasi-static conditions and higher bitumen percentages; 2) CR content increases damping properties.

3.6. Frequency versus time domain

In Figure 12, the comparison of the mechanical impedance in frequency and in time domain is illustrated.

The frequency-domain forces, $F(s)$, are obtained from time-domain forces in Newton, $f(t)$. In turn, $F(s)$ has units of N·s. Similarly, speeds in the frequency domain, $(V(s))$ with units of m are obtained from speeds in the time domain with units of m/s, $(V(t))$.

For all the methods, it has been noted that MI results in the time domain higher are than those derived in the frequency domain. On average, it can be summarized that (cf. Figure 13):
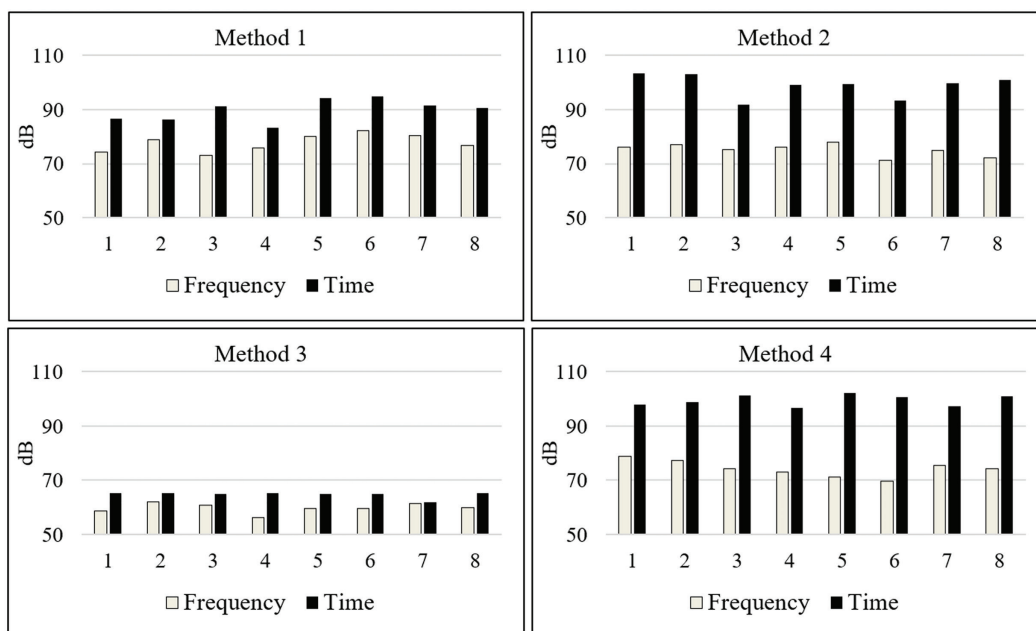
Figure 12. Comparison of Mechanical Impedance between frequency and time domain with the four methods used

Filippo G. Pratico,
Gianfranco Pellicano,
Matteo Bolognese,
Gaetano Licitra

A study
on frequency
response functions
in pavement
engineering

for Method 1, $F(s) = 0.87 * f(t)$ or $F(s) = f(t) - 12$ dB,
for Method 2, $F(s) = 0.76 * f(t)$ or $F(s) = f(t) - 24$ dB,
for Method 3, $F(s) = 0.92 * f(t)$ or $F(s) = f(t) - 5$ dB,
for Method 4, $F(s) = 0.75 * f(t)$ or $F(s) = f(t) - 25$ dB.

Discussion and conclusions

This study aimed at exploring the complexity of the applications of frequency response functions to asphalt concretes. The results obtained should be referred to the methods used, the main parameter selected (MI), the corresponding range of indicators explored (i.e., forces and accelerations), the devices selected (including the hammer), and the hypotheses formulated. Another factor that affects the results is that they refer to laboratory samples in order to highlight the potential of the method at the design stage. Additionally, it seems important to point out that equal drop heights correspond to the same energy but that this energy is spent in terms of strains that are mainly distributed among the hammer tip, impedance head (in the case of Method 3), and the sample. This implies that the same quantity of potential energy (hammer drop) may correspond to a different quantity of dissipated energy (as a result of sample strain). This is another factor that affects the actual time or frequency response as a function of output. Based on the results, the following conclusions can be drawn.
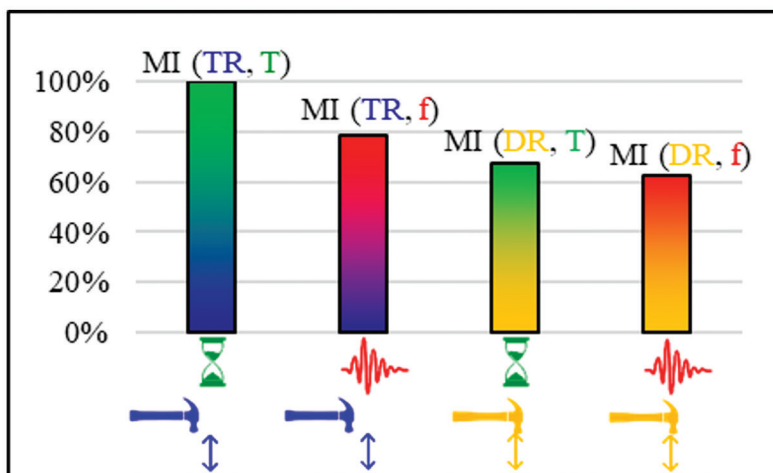
Symbols: MI: mechanical impedance; TR: transfer MI; DR: driving-point MI; T: time-domain MI; f: frequency-domain MI.

Figure 13. Simplified summary

For a given height, the force (sample-hammer) depends on two main factors, i.e., the type of the tip and the presence of the impedance head:

– Plastic tips generate higher forces while the use of the impedance head (coaxiality, i.e., the driving point) results in lower forces;

– The acceleration of the sample mainly depends on the tip material and coaxiality: plastic tips instigate higher accelerations, while accelerations are higher when measured under the hammer (coaxiality);

– The speed of the sample mainly depends on coaxiality (higher speeds under the hammer spot) and the type of tip material (higher speeds correspond to plastic tips);

    o The highest speeds are obtained with Method 3 (driving-point impedance), followed by Method 1, with the remaining methods giving very low speeds, bud this result is predictable due to the lower force impressed in Methods 2 and 4 compared to Method 1. Importantly, Method 3 is the coaxial one (accelerations were measured just under the hammer). This point seems quite reasonable and consistent with the previous analysis, because while forces are measured always under the hammer tip, in the case of Method 3, also the accelerations (and the speeds) are evaluated there (i.e., coaxially). Importantly, for speeds, the effect of the (null) distance prevails over the hardness of the tip;

    o The points above explain why Method 3 is the one that has the lowest MI. Indeed, measuring driving point MI, we expect higher velocity (or acceleration) at fixed input force;

    o Considering acceleration (acceleration/force) and stiffness (Force/Velocity) the results of Methods 2 and 4 are identical;

– MI (Mechanical Impedance) mainly depends on how F and V vary. Based on the above said, it turns out that Method 3, when coaxial speeds are considered, yields the lowest MIs. It is important to highlight here that comparing Method 3 with the remaining ones is partly questionable because Method 3 is conceptually different from the other methods (direct versus transmitted MI);

    o In more detail, using Method 3 (the load applied and the acceleration is measured at the same point through the impedance head) lower values of Mechanical Impedance are obtained. This is caused by higher values of velocity, as illustrated in Figure 11. On average, Method 3 (driving-point impedance) leads to MIs 20–55 times lower.

    o Comparing Methods 1, 2, and 4, the Mechanical Impedance appears to be quite the same in the range of 0–100 Hz, even if the force used with Method 1 is almost 5 times larger than the force of Method 2 and almost 10 times larger than the force of Method 4.

Filippo G. Pratico,
Gianfranco Pellicano,
Matteo Bolognese,
Gaetano Licitra

A study
on frequency
response functions
in pavement
engineering

This could suggest that the measurement of non-axial MI, which is not affected by the presence of the impedance head, is not force-dependent in that frequency range;

o   The highest force and acceleration pertain to Method 1, while the remaining methods yield lower results. This suggests that the type of tip is more important than the remaining factors when dealing with forces and accelerations. In more detail, it seems here very important to observe that Method 3 (coaxiality) yields the second level of acceleration. This leads to the conclusion that the material of the hammer tip is the most important factor and coaxiality is the second when dealing with accelerations. Indeed, in Method 1, greater forces cause greater accelerations, and these latter ones slightly decay. In contrast, in Method 3, forces are lowered by the different hammer tips but accelerations are measured just under the hammer tip. In other words, tip hardness and acceleration decay are concurring factors diversely affecting the measured accelerations;

o   In Method 2 and Method 4, the rubber tip and the nonaxial measurement of pavement response concur towards achieving lower forces, much lower speeds, and higher MIs.

−   For the dependency on crumb rubber, given the low percentages of crumb rubber, this could cause minor effects in terms of Mechanical Impedance (lower values, cf. Method 2, 5_0%CR_6.4%B vs. 6_2%CR_6.4%B). It seems that in 0–500 Hz the effect is quite negligible. Further studies are needed to address this topic;

−   For the dependency on bitumen percentage, results call for further studies and the considered range of bitumen percentage should be widened;

−   Under the given assumptions (distance between accelerometer – used for the transfer impedance – and the impedance head – used for the driving-point impedance – of about 2 cm), the driving-point impedance yields lower MIs (about 10–20 dB). It has been noted that this fact could depend on test geometry;

−   The Mechanical Impedance in the time domain is higher than the one derived from the frequency domain;

−   Results demonstrate that the ratio between the repeatability and the average is quite constant, while for heights higher than 10 cm, also MI tends to be independent of height;

−   Recommendations are as follows. In order to better use FRFs it is recommended: 1) to fix the height through a device; 2) to use heights higher than 10 cm; 3) to work on a comparative basis (comparing two situations); 4) to use the driving-point method (when moduli are not concerned) because of the appreciable dependence of the transfer

method on the distance hammer-accelerometer. This aspect calls for further research; 5) for research purposes, to model the system, for example, in terms of spring series.

– In terms of standardisation, different strategies could be adopted. It is envisaged that there may be different objectives and requirements when selecting or setting up a new standard. In terms of objectives, it appears very important to select the method that mostly represents the generation factors of the Van der Pol equation. In other terms, future studies should address the selection of the best indicator in terms of its ability to express acoustic pavement-tyre interaction. Having that in mind, this study can provide insights into the intrinsic characteristics of the methods investigated with the aim of minimising the corresponding acoustic power.

Funding information

Acknowledgement

REFERENCES

AASHTO M 323. (2017). *Standard specification for superpave volumetric mix design.* https://global.ihs.com/doc_detail.cfm?document_name=AASHTO%20M%20323&item_s_key=00488656

ASTM E965-15. (2019). *Standard test method for measuring pavement macrotexture depth using a volumetric technique.* https://doi.org/10.1520/E0965-15R19

Alani, H. M. H., Albayati, H. A., and Abbas, S. A. (2010). The transition to a PG grading system for asphalt cement in Iraq. *Journal of Engineering*, *16*(4), 5911–5931. https://www.iasj.net/iasj/download/c881cacd0e6cafdf

Bede, N., & Kožar, I. (2016). Determination of dynamic modulus of elasticity of concrete by impact hammer. *HDKBR INFO Magazin*, *6*(1), 8–11. https://hrcak.srce.hr/170434

Filippo G. Pratico,
Gianfranco Pellicano,
Matteo Bolognese,
Gaetano Licitra

A study
on frequency
response functions
in pavement
engineering

Bendtsen, H., Olesen, E., Pigasse, G., Andersen, B., Raaberg, J., Kalman, B., & Cesbron, J. (2013). *Measurements at the Arnakke test site with small PERS sections*. PERSUADE European Project, Seventh Framework Programme (Contract No. 226313- Measurement report).

Bocci, E., & Prosperi, E. (2020). Recycling of reclaimed fibers from end-of-life tires in hot mix asphalt. *Journal of Traffic and Transportation Engineering (English Edition)*, *7*(5), 678–687. https://doi.org/10.1016/j.jtte.2019.09.006

Brown, D. L., Allemang, R. J., & Phillips, A. W. (2015). Forty years of use and abuse of impact testing: A practical guide to making good FRF measurements. In J. De Clerck (ed.), *Experimental Techniques, Rotating Machinery, and Acoustics. Conference Proceedings of the Society for Experimental Mechanics Series*, *8*, (pp. 221–241). Springer, Cham. https://doi.org/10.1007/978-3-319-15236-3_21

Bruel & Kjaer. (2018). *Impact hammer - type 8206*. https://www.bksv.com/en/transducers/vibration/impact-hammers/8206

Buzdugan, Gh., Mihâilescu, E., & Rades, M. (1986). *Vibration measurement*. Springer Nature Customer Service Center LLC.

Cambpell, J. L., & Jurist, J. M. (1971). Mechanical impedance of the femur: a preliminary report. *Journal of Biomechanics*, *4*(5), 319–322. https://doi.org/10.1016/0021-9290(71)90052-2

Cesbron, J., Bianchetti, S., Pallas, M.-A., Praticò, F. G., Fedele, R., Pellicano, G., Moro, A., & Bianco, F. (2021). Acoustical characterization of low-noise prototype asphalt concretes for electric vehicles. *Euronoise 2021 Conference*. https://hal.science/hal-03423303/document

Clem, D. J., Popovics, J. S., Schumacher, T., Oh, T., Ham, S., & Wu, D. (2013). Understanding the impulse response method applied to concrete bridge decks. *AIP Conference Proceedings*, *1511*(1), 1333–1340. https://doi.org/10.1063/1.4789197

Coermann, R. R. (1962). The mechanical impedance of the human body in sitting and standing position at low frequencies. *Human Factors: The Journal of the Human Factors and Ergonomics Society*, *4*(5), 227–253. https://doi.org/10.1177/001872086200400502

Corliss, E. L. R., & Koidan, W. (1955). Mechanical impedance of the forehead and mastoid. *The Journal of the Acoustical Society of America*, *27*(6), 1164–1172. https://doi.org/10.1121/1.1908150

Czech, K. R., & Gardziejczyk, W. (2022). Investigation of the dynamic stiffness of poroelastic and asphalt concrete layers under in situ and laboratory conditions. *Materials*, *15*(5), Article 1821. https://doi.org/10.3390/ma15051821

de León, G., del Pizzo, A., Teti, L., Moro, A., Bianco, F., Fredianelli, L., & Licitra, G. (2020). Evaluation of tyre/road noise and texture interaction on rubberised and conventional pavements using CPX and profiling measurements. *Road Materials and Pavement Design*, *21*(sup1), S91–S102. https://doi.org/10.1080/14680629.2020.1735493

EN 12697-36. (2006). *Bituminous mixtures – Test methods for hot mix asphalt – Part 36: Determination of the thickness of a bituminous pavement.*

EN 13036-1. (2010). *Road and airfield surface characteristics. Test methods. Measurement of pavement surface macrotexture depth using a volumetric patch technique.*

EN 29052-1. (1992). *Acoustics – Method for the determination of dynamic stiffness – Part 1: Materials used under floating floors in dwellings.*

Fedele, R., Praticò, F. G., Carotenuto, R., & Della Corte, F. G. (2017). Instrumented infrastructures for damage detection and management. *5th IEEE International Conference on Models and Technologies for Intelligent Transportation Systems (MT-ITS).* Naples, Italy, 26–28 June 2017. https://doi.org/10.1109/MTITS.2017.8005729

Ferrari, P., & Giannini, F. (2000). *Ingegneria stradale – Corpo stradale e pavimentazioni* (1st ed.). Isedi.

Gatscher, J. A. & Kawiecki, G. (1994). *Mechanical Impedance Methods for Vibration Simulation.* American Institute of Aeronautics and Astronautics.

Gerdeen, J. W. (1975). *Mechanical impedance techniques applied to measuring the complex modulus of bone.* http://lib.dr.iastate.edu/rtd

Gil-Abarca A., Vázquez V. F., García-Hoz A. M., Terán F., & Paje S. E. (2021, October). Dynamic stiffness assessment of rubberized bituminous mixtures. *Euronoise 2021.*
http://www.sea-acustica.es/fileadmin/Madeira21/ID133.pdf

Griffin, M. J. (2001). Whole-body vibration. *Encyclopedia of Vibration*, *2001*, 1570–1578. https://doi.org/10.1006/rwvb.2001.0082

Gucunski, N., Imani, A., Romero, F., Nazarian, S., Yuan, D., Wiggenhauser, H., Shokouhi, P., Taffe, A., & Kutrubes, D. (2013). *Nondestructive testing to identify concrete bridge deck deterioration.* National Academies of Sciences, Engineering, and Medicine. The National Academies Press.
https://doi.org/10.17226/22771

Hamet, J.-F., & Klein, P. (2004). *Road stiffness influence on rolling noise: Parametric study using a rolling tire model.*
https://hal.archives-ouvertes.fr/hal-00546101

Harris, C. M., Piersol, A. G. (2002). *Harris' shock and vibration handbook.* McGraw-Hill.

ISO 5725-1. (1994). *Accuracy (trueness and precision) of measurement methods and results: General principles and definitions.*

Kweon, G., & Kim, Y. R. (2006). Determination of asphalt concrete complex modulus with impact resonance test. *Transportation Research Record: Journal of the Transportation Research Board*, *1970*(1), 151–160.
https://doi.org/10.1177/0361198106197000116

Li, M., Molenaar, A. A. A., van de Ven, M. F. C., & van Keulen, W. (2012). Mechanical impedance measurement on thin layer surface with impedance hammer device. *Journal of Testing and Evaluation*, *40*(5), Article 20120089. https://doi.org/10.1520/jte20120089

Li, M., van Keulen, W., Ceylan, H., Cao, D., van de Ven, M., & Molenaar, A. (2016). Pavement stiffness measurements in relation to mechanical impedance. *Construction and Building Materials*, *102*(1), 455–461.
https://doi.org/10.1016/j.conbuildmat.2015.10.191

Filippo G. Pratico,
Gianfranco Pellicano,
Matteo Bolognese,
Gaetano Licitra

A study
on frequency
response functions
in pavement
engineering

Merenda, M., Praticò, F. G., Fedele, R., Carotenuto, R., & della Corte, F. G. (2019). A real-time decision platform for the management of structures and infrastructures. *Electronics*, *8*(10), Article 1180. https://doi.org/10.3390/electronics8101180

Mizrahi, J. (2015). Mechanical impedance and its relations to motor control, limb dynamics, and motion biomechanics. *Journal of Medical and Biological Engineering*, 35(1), 1–20. https://doi.org/10.1007/s40846-015-0016-9

Morcillo, M. A., Hidalgo, M. E., Pastrana, M. del C., García, D., Torres, J., & Arroyo, M. B. (2019). Life Soundless: New generation of eco-friendly asphalt with recycled materials. *Environments*, *6*(4), Article 48. https://doi.org/10.3390/environments6040048

Mun, S. (2015). Determining the dynamic modulus of a viscoelastic asphalt mixture using an impact resonance test with damping effect. *Research in Nondestructive Evaluation*, *26*(4), 189–207. https://doi.org/10.1080/09349847.2015.1023914

Olesen, H. P. (1972). Measurement of the Dynamic Properties of Materials and Structures, Brüel & Kjær Application Notes. https://www.bksv.com/media/doc/17-180.pdf.

Olesen, H. P., Randall, R. B. (1979). A Guide to Mechanical Impedance and Structural Response Techniques Structural Response Techniques, Brüel & Kjaer Application Note 17-179.

Oyadiji, S. O., & Tomlinson, G. R. (1994). Relating the complex moduli of viscoelastic materials to the complex stiffness of antivibration mounts. *Proc. SPIE 2193, Smart Structures and Materials 1994: Passive Damping*, C. D. Johnson (ed.), *2193*, 226–237. https://doi.org/10.1117/12.174099

Pimentel, R., Guedes, T., Melo, L., Ferreira, G., & Gonçalves, M. (2017). Damage detection assessment in reinforced concrete slabs using impact tests. *Procedia Engineering*, *199*, 1976–1981. https://doi.org/10.1016/j.proeng.2017.09.307

Policarpo, H., Neves, M. M., Luis, J., Coelho, B., Neves, M. M., Maia, N. M. M., Bento Coelho, J. L., Gerges, S. N. Y., & Viveiros, E. (2010). On the determination of dynamic properties of resilient materials using a multilaminated periodic specimen. *17th International Congress on Sound and Vibration*. https://www.researchgate.net/publication/235911170_On_the_determination_of_dynamic_properties_of_resilient_materials_using_a_multilaminated_periodic_specimen

Praticò, F. G. (2007). Quality and timeliness in highway construction contracts: A new acceptance model based on both mechanical and surface performance of flexible pavements. *Construction Management and Economics*, *25*(3), 305–313. https://doi.org/10.1080/01446190601042426

Praticò, F. G., Fedele, R., & Pellicano, G. (2021a). *Monitoring Road Acoustic and Mechanical Performance*. In P. Rizzo, & A. Milazzo (Eds.), *European Workshop on Structural Health Monitoring. EWSHM 2020. Lecture Notes in Civil Engineering*, *127* (pp. 594–602). Springer, Cham. https://doi.org/10.1007/978-3-030-64594-6_58

Praticò, F. G., Fedele, R., & Pellicano, G. (2021b). Pavement FRFs and noise: A theoretical and experimental investigation. *Construction and Building Materials*, *294*, Article 123487.
https://doi.org/10.1016/j.conbuildmat.2021.123487

Praticò, F. G., Pellicano, G., & Fedele, R. (2021c, October 25). Low-noise road mixtures for electric vehicles. *EuroNoise 2021*.

Praticò, F. G., & Vaiana, R. (2012). Improving infrastructure sustainability in suburban and urban areas: Is porous asphalt the right answer? And how? *WIT Transactions on the Built Environment*, *128*, 673–684.
https://doi.org/10.2495/UT120571

Radenberg, M., Drewes, B., & Manke, R. (2017). Noise reducing effect of new dense asphalt layers. *6th Eurasphalt & Eurobitume Congress,* Prague, Czech Republic.

Schubert, S., Gsell, D., Steiger, R., & Feltrin, G. (2010). Influence of asphalt pavement on damping ratio and resonance frequencies of timber bridges. *Engineering Structures*, *32*(10), 3122–3129.
https://doi.org/10.1016/j.engstruct.2010.05.031

Shell International Petroleum Company Limited. (1978). *Shell pavement design manual: Asphalt pavements and overlays for road traffic*. Shell International Petroleum.

Skov, R. S. H., Bendtsen, H., Raaberg, J., & Cesbron, J. (2015). Laboratory measurements on slabs from full scale PERS test sections. *EuroNoise 2015*, 1339–1344. https://www.conforg.fr/euronoise2015/proceedings/data/articles/000421.pdf

Smith, S. D., & Kazarian, L. E. (1994). The effects of acceleration on the mechanical impedance response of a primate model exposed to sinusoidal vibration. *Annals of Biomedical Engineering*, *22*, 78–87.
https://doi.org/10.1007/BF02368224

Strivens, T. A. (1999). The rheology of paints. In *Paint and Surface Coatings* (2nd ed., pp. 575–597). Elsevier. https://doi.org/10.1533/9781855737006.575

Suggs, C. W., & Abrams, C. F. (1971). Mechanical impedance techniques for evaluating the dynamic characteristics of biological materials. *Journal of Agricultural Engineering Research*, *16*(3), 307–315.
https://doi.org/10.1016/S0021-8634(71)80022-7

Tlaisi, A. A., Swamidas, A. S., Akinturk, A., & Haddara, M. R. (2012). Crack detection in shafts using mechanical impedance measurements. *Mechanical Engineering Research*, *2*(2), 10–30. https://doi.org/10.5539/mer.v2n2p10

van Velsor, J. K., Premkumar, L., Chehab, G., & Rose, J. L. (2011). Measuring the complex modulus of asphalt concrete using ultrasonic testing. *Journal of Engineering Science and Technology Review*, *4*(2), 160–168.
https://doi.org/10.25103/jestr.042.08

Vázquez, V. F., & Paje, S. E. (2015). Dynamic stiffness assessment of bituminous mixtures type SMA according construction characteristics. *The 22nd International Congress on Sound and Vibration (ICSV22)*. Florence, Italy. 12–16 July 2015.

Filippo G. Pratico,
Gianfranco Pellicano,
Matteo Bolognese,
Gaetano Licitra

A study
on frequency
response functions
in pavement
engineering

Notations

m – mass;
c – viscous damping coefficient;
k – spring constant;
$\ddot{x}$ – acceleration;
$\dot{x}$ – speed;
x – displacement;
$f(t)$ – force in time domain;
$F(s)$ – force in frequency domain;
ω – angular frequency;
ω_n – resonant angular frequency;
ζ – damping ratio;
$G_{mb\ DIM}$ – bulk specific gravity calculated considering the dimensions and
weight of the sample;
AC6 – Asphalt Concrete with Nominal Maximum Aggregate Size of 6 mm;
D – diameter;
t – thickness;
W – weight;
$G_{mb\ COR}$ – bulk specific gravity measured using the Corelok machine;
AV_{COR} – air void content measured using the Corelok machine;
F_{max} – max force;
A_{max} – max acceleration;
V_{max} – max velocity;
D_{max} – max displacement;
M – average;
St.dev.s – sample standard deviation;
r – repeatability.

Abbreviations

FRF – Frequency Response Function
MI – Mechanical Impedance
IR – Impulse Response
NDT – Non-Destructive Test
CR – Crumb Rubber
AR – Acoustic Response
PERS – Poroelastic Road Surface
RT – Rubber Tip

PT – Plastic Tip
CH – Controlled Height
CF – Controlled Force
NA – Nonaxial
CA – Coaxial
FFT – Fast Fourier Transform
B – Bitumen
UCR – Untreated Crumb Rubber
MTD – Mean Texture Depth